nature physics

SUPPLEMENTARY INFORMATION

https://doi.org/10.1038/s41567-020-0809-9

In the format provided by the authors and unedited.

Chromatic neuronal jamming in a primitive brain

Margarita Khariton[1,4], Xian Kong[2,4], Jian Qin[2]✉ and Bo Wang[1,3]✉

[1]Department of Bioengineering, Stanford University, Stanford, CA, USA. [2]Department of Chemical Engineering, Stanford University, Stanford, CA, USA. [3]Department of Developmental Biology, Stanford University School of Medicine, Stanford, CA, USA. [4]These authors contributed equally: Margarita Khariton, Xian Kong. ✉e-mail: jianq@stanford.edu; wangbo@stanford.edu

Supplementary Information

‘Chromatic’ Neuronal Jamming in a Primitive Brain

Margarita Khariton[1,4], Xian Kong[2,4], Jian Qin[2,*], Bo Wang[1,3,*]

[1]Department of Bioengineering, Stanford University, Stanford, CA, USA. [2]Department of Chemical Engineering, Stanford University, Stanford, CA, USA. [3]Department of Developmental Biology, Stanford University School of Medicine, Stanford, CA, USA.
[4]These authors contributed equally to this work.

Contents

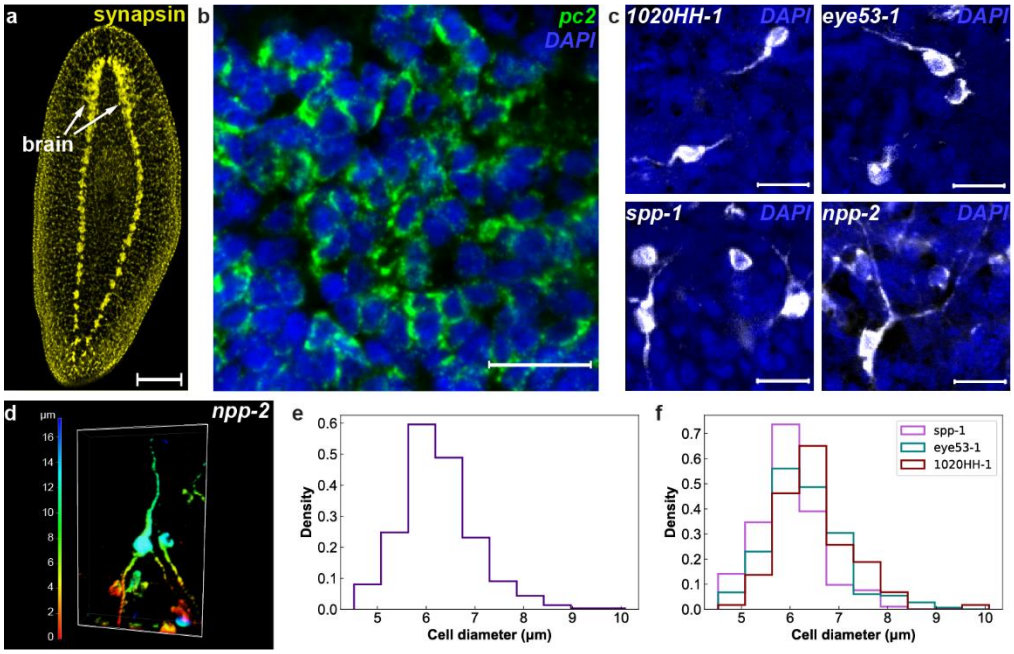

Supplementary Figure 1. The planarian central nervous system. a) Two cephalic ganglia in the anterior constitute dense synapses, stained by anti-synapsin (antibody 3C11, Developmental Studies Hybridoma Bank). **b)** *pc2* is expressed in all peptidergic neurons, which comprise a major population of the neuronal cells in the planarian brain[27]. *pc2* mRNA is visualized by FISH; DAPI stains the nucleus. Only a subset of cells in the image view express *pc2*, as the planarian brain also contains numerous non-peptidergic neuronal types, intermixed with other non-neuronal cell types, such as glia, along with extracellular structures[35-37]. Earlier ultrastructural studies have also observed muscle fibers and parenchymal cytoplasmic processes in the interneuronal space[35,43]. As homotypic repulsion is mediated through a variety or combination of diffusive cues and long neuronal processes, the complex tissue structure and cellular composition of the brain should induce the interaction to have a range of length scales, which is consistent with the broad distributions of the size of homotypic packing units (**Fig. 2c**). **c)** FISH images of individual neurons, depicting their relative densities, cell body shapes, and processes that can extend several cell body sizes. **d)** 3D render of *npp-2*$^{+}$ neurons showing their spherical volume and long extensions. **e)** Planarian neuronal cells are relatively homogenous in size: distribution of cell body sizes presents as a sharp peak centered about a mean of 6.25 ± 0.76 μm cell diameter, as measured in FISH images across 537 *1020HH-1*$^{+}$, *eye53-1*$^{+}$, and *spp-1*$^{+}$ cells in four animals. **f)** This distribution is independent of cell type. The particularly small deviation in cell body size should not affect the long-range interactions. Scale bars: **a**) 200 μm, **b-c**) 20 μm.

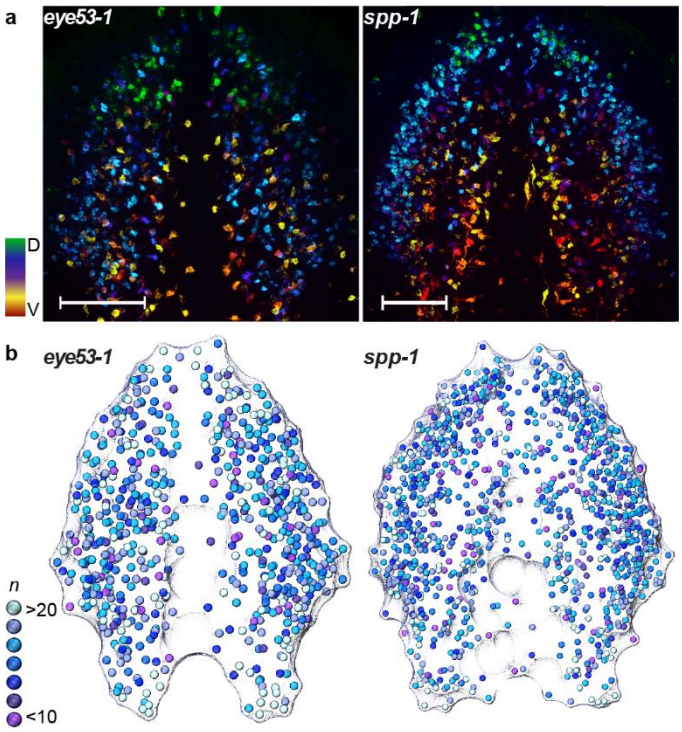

Supplementary Figure 2. Single-neuron resolution of multiple peptidergic neuronal types in the planarian brain. a) Depth-colored projection images showing RNA-FISH of neuropeptides *eye53-1* (left) and *spp-1* (right) to reveal spatial distributions of *eye53-1*$^{+}$ and *spp-1*$^{+}$ peptidergic neurons, respectively, in the planarian brain. Colormap: dorsal-to-ventral. Scale bars: 100 μm. **b)** Centroids of *eye53-1*$^{+}$ (left) and *spp-1*$^{+}$ (right) peptidergic neurons corresponding to images in **a**. Colors represent number of nearest homotypic neighbors (*n*) of each individual neuron, determined by Voronoi tessellation.

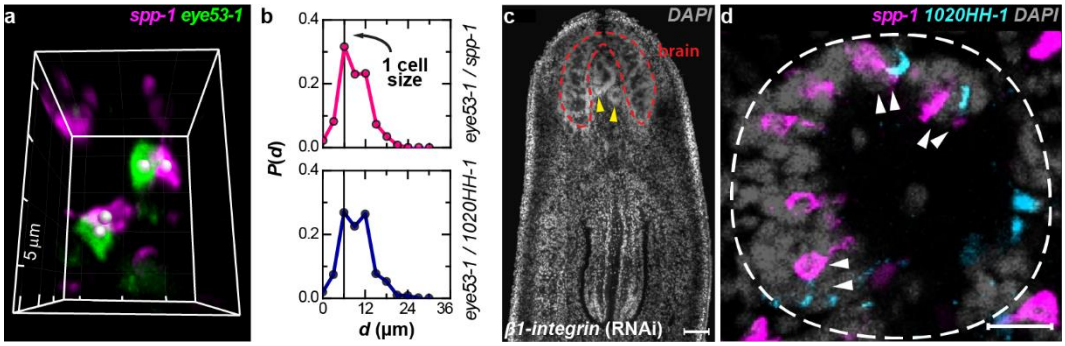

Supplementary Figure 3. Repulsion is not observed between heterotypic neuronal types. a) 3D reconstruction image showing that *spp-1*$^+$ (magenta) and *eye53-1*$^+$ (green) neurons can locate in physical proximity. Grey: cell body centroids. **b)** Probability distributions of separation between closest pairs of heterotypic neurons for 3 representative peptidergic neuronal types: *eye53-1*$^+$ */ spp-1*$^+$ (top) and *eye53-1*$^+$ */ 1020HH-1*$^+$ (bottom). Statistics on heterotypic pairs were obtained by analyzing 4 planarians each. Distributions peak around 6 µm, equivalent to one cell size, suggesting heterotypic neurons often form physical contacts. **c)** To confirm that inter-neuronal spacing is controlled by local cell-cell interactions rather than global patterning cues that may be specific to the brain tissue, neuronal organization is characterized in ectopic neuronal aggregates (yellow arrowheads). Ectopic neural spheroids are induced by knockdown of *β1-integrin* using RNA interference (RNAi) as reported previously[39,40]. β-integrin is known to mediate cell-ECM interactions and cell migration, yet disrupting its function does not change the packing pattern of the homotypic neurons even in ectopic neural spheroids. This observation is consistent with a recent study that has knocked down the primary components of ECM in planarians and reported no neural phenotypes[44]. Scale bar: 100 µm. **d)** A representative spheroid (dashed circle) is shown to illustrate that heterotypic neurons (*spp-1*$^+$ and *1020HH-1*$^+$ peptidergic neurons) can locate in physical proximity to form dimers (white arrowheads), whereas homotypic neurons are always separate in space. This data is consistent with homotypic repulsion, even in this ectopically induced neural mass outside of the brain. Scale bar: 20 µm.

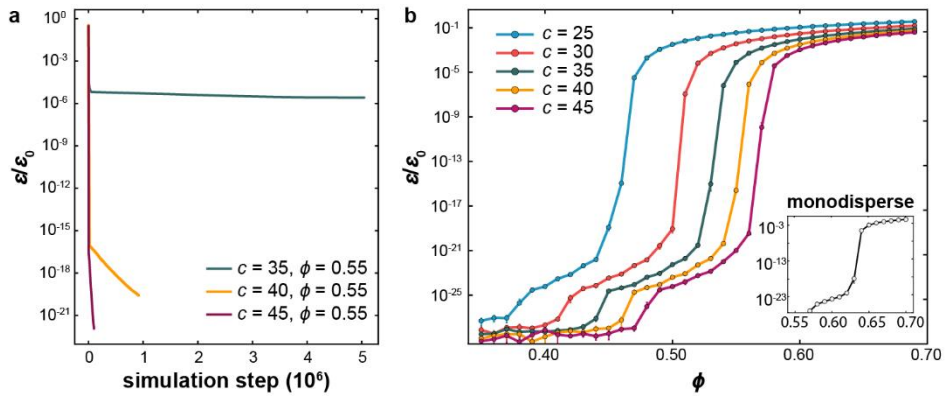

Supplementary Figure 4. System energy defines the jamming transition. a) Residual energy per particle (ε) evolution during the energy minimization equilibration for several color numbers (c) at a fixed packing fraction (ϕ). Simulations were terminated when energy change between consecutive steps dropped below a tolerance of $10^{-20}\,\varepsilon_0$. **b)** Minimum residual energy per particle (ε) versus ϕ for varying c. The J transition is defined at critical ϕ when the steepest increase in energy of each condition is identified. Inset: energy residual varying with ϕ in a monodisperse system. The steepest energy jump occurs near the well-defined jamming point[17,19] of $\phi_s = 0.64$. Error bars represent standard deviation.

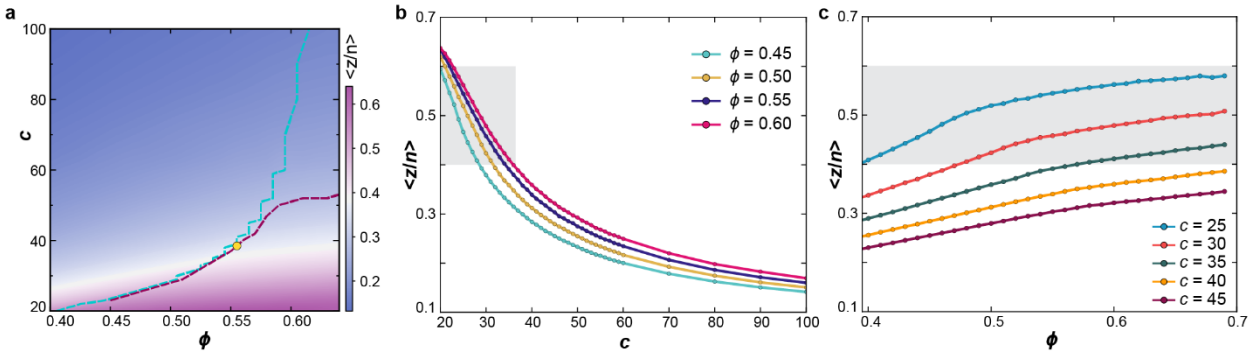

Supplementary Figure 5. The average fraction of contact neighbors, ⟨*z*/*n*⟩, of homotypic neighbors depends strongly on color number but weakly on packing density. a) Heatmap depicting ⟨*z*/*n*⟩ of the model as a function of *c* and ϕ. Cyan line: J transition; red line: P transition. **b)** Simulated ⟨*z*/*n*⟩ is plotted against *c* for varying ϕ. **c)** ⟨*z*/*n*⟩ is plotted against ϕ for varying *c*. Note that, in conventional jamming models, ⟨*z*/*n*⟩ is expected to be a function of packing density[17,19]. Grey zones specify the regime observed in experiments.

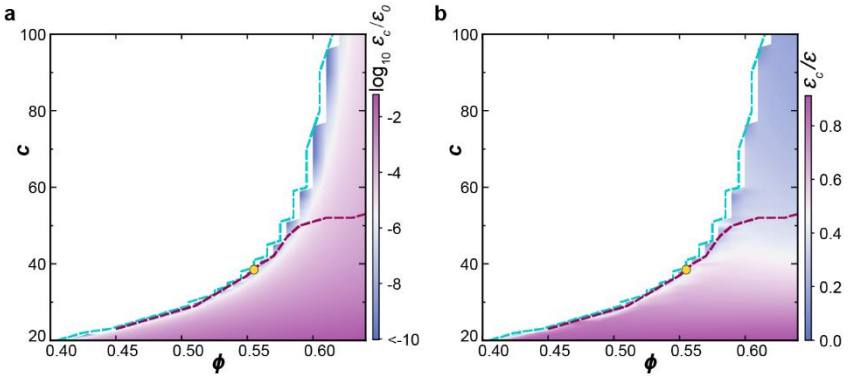

Supplementary Figure 6. Energy contribution of homotypic interactions increases as color number decreases. a) Heatmap showing the residual energy per particle due to homotypic interactions as a function of c and ϕ. **b)** Heatmap depicting the fraction of total energy that arises from homotypic interactions, as a function of c and ϕ. Cyan line: J transition; red line: P transition.

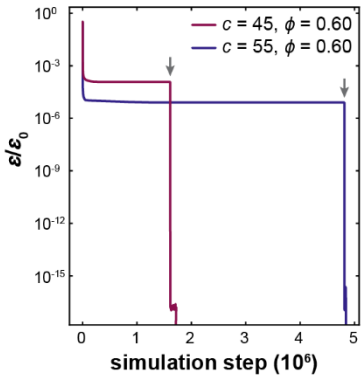

Supplementary Figure 7. Homotypic interaction underlies chromatic jamming in the colored particle model. Residual energy per particle (ε) evolution during the energy minimization equilibration after turning off homotypic interaction. With homotypic interaction, both systems are jammed, one with homotypic percolation (c = 45, ϕ = 0.60, red line) and the other without homotypic percolation (c = 55, ϕ = 0.60, blue line). Both systems exhibit mechanical stability: at (ϕ, c) = (0.60, 45), the bulk modulus is 0.489±0.003 ε_0/σ_0^3 and the shear modulus is 0.084±0.009 ε_0/σ_0^3; at (ϕ, c) = (0.60, 55), the bulk modulus is 0.385±0.005 ε_0/σ_0^3 and the shear modulus is 0.041±0.009 ε_0/σ_0^3. After turning off homotypic repulsion (gray arrows), both systems become unjammed with ε = 0 (which cannot be shown on a log scale plot) after relaxation.

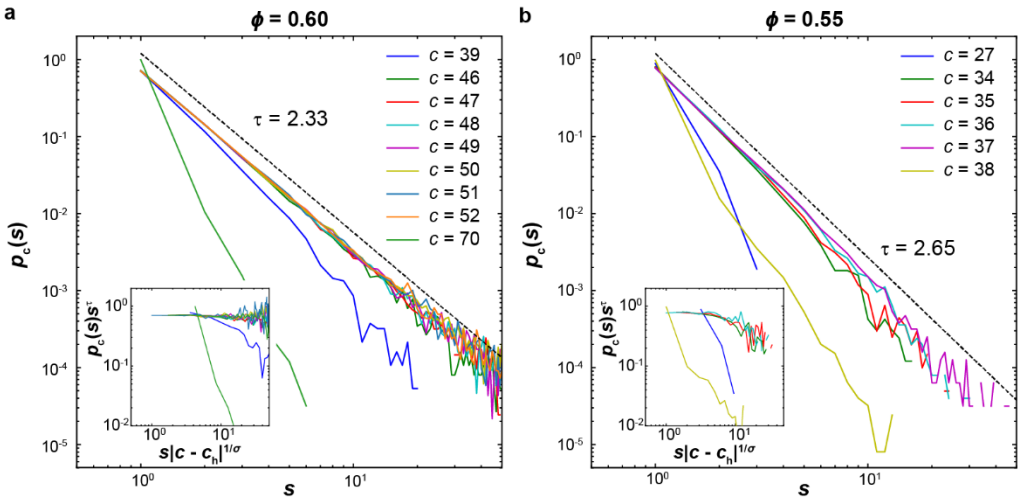

Supplementary Figure 8. Power-law cluster size distribution defines the percolation transition. Cluster size distributions at two packing densities, **a)** ϕ = 0.60, and **b)** ϕ = 0.55, flanking the triple point (ϕ*, c*) = (0.56, 40). Distributions with several color numbers near the critical color number (c_h) are shown; the percolation transition is defined when the power-law distribution spans the widest range of s. For comparison, two cases far away from c_h are shown as divergent from the power law. Dashed lines: asymptotic power law with exponent τ specified. τ is consistent with 3D percolation theory[34]. Inset: the collapse of cluster distributions as $p_c(s)s^\tau$ is plotted against $s|c\text{-}c_h|^{1/\sigma}$ with corresponding τ and σ = 2. Note that, when $\phi > \phi$*, the power-law distribution is robust throughout broad ranges of color numbers around c_h, whereas the power law only exists in narrower ranges as $\phi < \phi$* and bends down at large cluster sizes. Moreover, τ remains nearly constant when $\phi > \phi$*. Below ϕ*, even though an analogous exponent τ can still be determined for finite clusters, it grows steadily as ϕ decreases. Why τ deviates from the classic value below ϕ* remains a subject of future study.

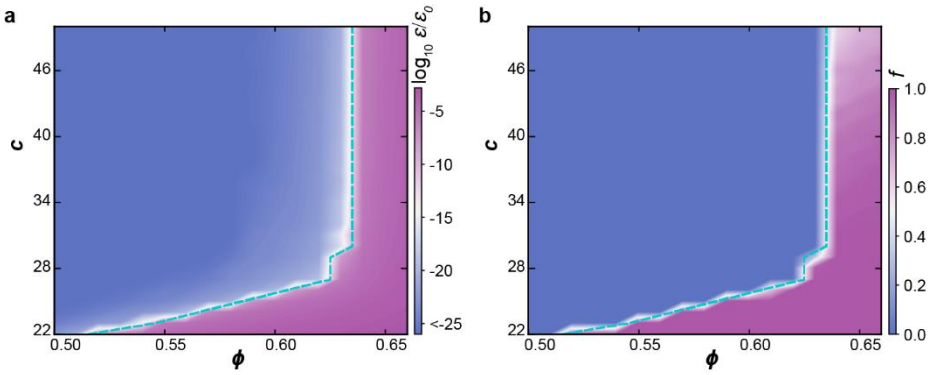

Supplementary Figure 9. Chromatic jamming in a binary model. a) Heatmap showing residual energy per particle after equilibration as a function of c and ϕ in a system containing two particle types, only one of which experiences homotypic repulsion. Cyan line: J transition. **b)** Heatmap showing the fraction of particles belonging to the largest homotypic cluster (f) as a function of c and ϕ. Note that the jamming and percolation transitions overlap when $\phi < 0.64$, the classical jamming point of unicomponent systems.

Supplementary Note 1: Homotypic repulsion.

It is self-evident that the distribution of neurons in any neural tissue must be tightly regulated through molecular cues specifying the identities of cells that surround any given cell[9,10]. These cell type-specific interactions can be mediated by diffusive factors that are recognized by cells at a distance or through cell surface receptors distributed along extended cellular processes. Upon recognition, homotypic cells and their processes respond to repellent forces with shape adjustment, migration, or growth behaviors. Indeed, diverse molecular mechanisms may be involved, as shown across a variety of nervous systems, including those of *Drosophila*, mouse, and *C. elegans* (e.g., TGF-b/Activin through diffusive signals as well as transmembrane cadherin Flamingo, immunoglobulin superfamily cell adhesion molecules (IgCAMs), and integrins mediating cell-cell adhesion, among others)[10,11,23]. The roles which these molecules and proteins may play during planarian neuronal packing and network formation, if any, is not yet known. However, the means by which homotypic interactions occur does not affect the characterization and understanding of neuronal packing, as it is an emergent problem that exists on a length scale much larger than specific molecular interactions, as supported by previous work in the field[8,9,22].

Although the exact mechanism controlling homotypic repulsion among planarian neurons remains to be uncovered, many key players of homotypic interactions (e.g., protocadherins, IgCAMs, and integrins) are known to be deeply conserved in the planarian[39,40,45]. For example, neuronal spacing in the fly and mouse visual systems is known to be mediated by homotypic repulsion through Down syndrome cell adhesion molecule (DSCAM), a member of the IgCAM superfamily[11,22]. Homologs of IgCAMs, including DSCAM and neural cell adhesion molecule (NCAM), are known to be present in the planarian central nervous system, with functional analyses showing them as playing key roles in neuronal interactions[45].

While such a mechanism is not required to understand the generic physical principles underlying cellular packing on a global level, new methodology must be developed in order to disrupt cellular packing, as existing experimental techniques lack the needed resolution. Selective ablation of a single neuron and specific disruption of homotypic interactions, for instance, are not possible in the planarian, and thus we cannot control precisely the perturbation of the jammed system to observe how it might rearrange. The toolbox of available assays in the planarian system is limited: our experiments here are based on fluorescent imaging of mRNA in fixed tissues, as we cannot perform neuronal imaging of these cell types on live worms. Thus we are unable to track dynamics of the perturbed system within the same worm to identify rearrangement. In addition, the outcome of tissue ablation in the planarian is quite complicated, as non-neuronal cells (e.g., glia) are recruited to the wound site as a response to injury. Disentangling the effects of wound healing response and neuronal repulsion or rearrangement would be problematic. Finally, when we knocked down conserved molecular components that mediate homotypic repulsion in other animals (e.g., DSCAM), we observed randomized distributions of homotypic neurons – they formed large clusters that contained many homotypic neurons in direct physical contact, yet these results were difficult to interpret as the same knockdown also perturbed the overall size and shape of the brain. This observation impeded our ability to make the appropriate geometric measurements of cellular distributions.

Therefore, we have taken an alternative approach often used to deal with particularly complex systems: build a system with reduced complexity, taking into account only the factors

of interest, and observe if this is sufficient to reproduce the phenomena observed in physical reality. We constructed such a model computationally, considering only homotypic repulsion, and show that it is sufficient to generate all of the observed statistical regularities. It would be powerful to ultimately increase the model's complexity layer-by-layer as the biological toolbox expands, or even to construct engineered cell lines with synthetic homotypic interactions in order to rebuild the homotypic jamming pattern *in vitro*.

Supplementary References

43. Sarnat H. B. & Netsky M. G. The brain of the planarian as the ancestor of the human brain. *Can. J. Neurol. Sci*. **12**, 296–302 (1985).
44. Cote, L. E., Simental, E. & Reddien, P. W. Muscle functions as a connective tissue and source of extracellular matrix in planarians. *Nat. Commun.* **10**, 1592 (2019).
45. Fusaoka, E., Inoue, T., Mineta, K., Agata, K. & Takeuchi, K. Structure and function of primitive immunoglobulin superfamily neural cell adhesion molecules: A lesson from studies on planarian. *Genes to Cells* **11**, 541–555 (2006).